Radiant, convective and heat release characterization of vegetation fire

Frédéric Morandini, Yolanda Perez-Ramirez, Virginie Tihay, Paul Antoine Santoni, Toussaint Barboni

Radiant, convective and heat release characterization of vegetation fire

Frédéric Morandini*, Yolanda Perez-Ramirez, Virginie Tihay, Paul-Antoine Santoni, Toussaint Barboni

SPE– UMR 6134 CNRS, University of Corsica, Campus Grimaldi, BP 52, 20250 Corte, France

Corresponding author: Frédéric Morandini

Phone: +33 495 450 243, Fax: +33 495 450 162,

E-mail address: frederic.morandini@univ-corse.fr

Abstract

Fire spread across forest fuel is usually characterized by the rate of spread or the fireline intensity. The determination of the fireline intensity represents an essential aspect for understanding the behaviour of the fire and the involved combustion processes. The heat released during fire spread cannot be a-priori estimated from the fundamental properties of the fuel material and experiments need to be carried out to determine it. This paper presents a global characterization of horizontal fire spread in still air across fuel beds in terms of heat release, rate of spread, flame geometry and radiant and convective fractions. The influence of the fuel load on these main fire properties is investigated. A series of experiments was conducted using a Large Scale Heat Release apparatus. The fire tests were carried out on a combustion table located on a load cell. The fuel consisted in a 2 m long and 1 m wide bed of pine needles. The fireline intensity was accurately estimated by means of oxygen consumption calorimetry and some other methods to assess this quantity were also tested. Combustion efficiency and effective heat of combustion were discussed. The heat fluxes emitted during the fire spread were also investigated. In the studied configuration, radiation was the dominant heat transfer mechanism in the preheating zone; whereas some transfers combining

radiation and convection were highlighted closer to the flame front. The radiant (from flame and embers) and convective fractions of the fire front were then calculated. The data exhibit that the fuel load has a significant influence on the thermal degradation of the forest material and on the resulting fire properties. The results also suggest that the measurement of the mass loss rate can be a good alternative to estimate accurately the fireline intensity when the measure of oxygen consumption is not possible like in field-scale scenarios.

Keywords: Heat release rate; Byram's intensity; Mass loss rate; Heat fluxes; Radiant and convective fractions.

Nomenclature

A	Cross sectional area of the exhaust duct
$c_{p,\,mix}$	Specific heat of the mixture
d	Duct diameter (0.4 m)
E	Heat of combustion
F	view factor
h	Fuel height
H	Heat yields
Hf	Flame height
HRR	Heat release rate
I	Fireline intensity
k_t	Constant determined via a propane burner calibration

k_p	Constant of the bi-directional probe (1.108)
Lf	Flame length
m	Mass of the fuel
$\dot{m}'$	Mass loss rate per unit length of fire front
$\dot{M}_{mix}$	Mass flow rate of the chemical compounds-air mixture
MLR	Mass loss rate
$\dot{n}^{\circ}_{O_2}$	Molar flow rates of O_2 in incoming air
$\dot{n}_{O_2}$	Molar flow rates of O_2 in the exhaust duct
q	Radiant heat flux density
S	Emission surface
T	Temperature
p_m	Moisture content of fuel
r	Rate of spread
T_s	Smoke temperature in the duct
U	Overall heat transmission coefficient of the duct
$\dot{V}_{s,298}$	Standard flow rate in the exhaust duct at 298 K
w	Mass of fuel consumed per unit area
W	Molecular weight
X	Molar fraction

Greek symbols

α	Expansion factor for the fraction of the air that was depleted of its oxygen
χ_{eff}	Combustion efficiency
χ_{rad}	Radiant fraction of the flame
χ_{conv}	Convective fraction
$\Delta H_{c,net}$	Net heat of combustion
ΔP	Pressure drop across the bi-directional probe
Φ_{loss}	Heat losses
ρ	Density of the fuel particles
ρ_0	Density of dry air at 298 K and 1 atm
σ	Surface to volume ratio of the fuel particles

Subscript

a	ambient
g	gas at duct entry
O2	Oxygen
N2	Nitrogen
CO2	Carbon dioxide
H_2O	Water vapour

Superscript

°	Incoming air
a	Ambient

1 Introduction

The concept of fireline intensity was introduced by Bryam in 1959 [1] and represents the heat released per unit time per unit length of the fire front (kW/m). Byram defined it as the product of the weight of fuel consumed per unit area (kg/m^2), the heat yield of the fuel (average value assumed to be 18 000 kJ/kg for most vegetative fuel) and the rate of spread (m/s), but this relation is only suitable for the ideal case of linear fire front spreading under quasi-steady conditions. More generally, the fireline intensity can be defined as the product of the rate of fuel consumption per unit length of fire front (kg/s/m) with the heat of combustion (fuel heat yield, kJ/kg). This last definition is convenient for both steady and unsteady fire spread. Fireline intensity is a key parameter when dealing with wildfires suppression, risk and potential damage since it incorporates several factors of the fire environment into a single number [2]. Thus, this quantity is widely used in forest fire science since it helps to evaluate the effects of fuel treatment on fire behavior, to establish limits for prescribed burning, and to assess fire impacts on ecosystems. Moreover, it is also used as an indicator for the classification in terms of risk and as a quantitative basis to support fire suppression activities.

Although it is a fundamental variable for understanding the fire behaviour, few studies have investigated the fireline intensity [3] even at laboratory scale and small number of methods has been developed to measure it [4]. Furthermore, the fireline intensity has nevertheless rarely been used as a key quantity to test the predictions of the fire spread models. These predictions are most often compared to some coarse observations of the fire front, such as rate of spread and flame geometric properties, or fire temperatures. The reason of this non-use of this property of the fire front to validate the models may be found in the difficulty encountered to estimate it accurately in the field

since there is no direct measurement instrument at that scale. Indeed, although the experiments at field scale [5] are valuable, the indirect estimation of fireline intensity at that scale is subject to errors, since it is computed from other quantities (mass of fuel consumed, rate of spread, etc). Thus, little is known about how well these estimations of fireline intensity represent the effective rate of energy release due to the uncertainties in measuring each quantity. For instance, the mass of the fuel consumed by the fire depends on the characteristics of the vegetation (species, size and distribution of solid particles, moisture content, packing ratio, quantity of duff and litter). This large number of factors greatly influences the fire behaviour [6]. Conversely, the experiments conducted at laboratory scale, with a greater control of the properties of the vegetative fuel, allow accurate measurements of the fire properties (rate of spread, flame geometry, heat release, heat transfers, mass loss, etc.). These small scale experiments are also devoted to the search and the development of methods and techniques for field applications.

Another aspect that deserves mention in the characterisation of spreading fires is the quantification of the radiant and convective fractions of the total heat release. Indeed, radiative and convective heat transfers play complementary roles in fire spread and it is necessary to understand how energy is released. Several studies have reported measurements of radiant or total heat transfers focussing on the heat flux that has an impact on the fuel ahead of a fire front [7-11]. Morandini and Silvani [10] showed the existence of two different regimes of fire spread (plume-dominated and wind-driven) that were either dominated by radiation or governed by mixed radiant–convective heat transfer; but quantifying their proportion remains difficult. Other studies [12-14] have focussed on the percentage of total energy released as radiation and convection. The measurements obtained by Knight and Dando [12] on a bushfire exhibit radiant fraction close to 20 %. Freeborn [13] and Kremens [14] performed middle infrared measurements using radiometers to determine the fire radiative energy and found radiant fraction of 12.4 % and 17 %, respectively. Freeborn [13] also suggested a convective fraction of about 52%. Tewarson [15] determined the convective fraction by using the Gas Temperature Rise (GTR) calorimetry. For pine wood, a convective fraction of 48.6 %

was found, which leads to a radiant fraction equal to 20.7%. In most of these studies, the authors assumed a complete combustion using the heat of combustion which introduces uncertainties in the estimation of the total heat released.

The present study focuses on the characterization of fires spreading across beds of fuel from a point of view of heat release and radiant and convective fractions. The method used for the measurement of the fireline intensity from oxygen consumption calorimetry (OCC) has already been detailed and tested for different fuels species [16]. The procedures to calibrate the apparatus and the estimation of the uncertainties (since the HRR is computed from many measured variables which have corresponding uncertainties) were also provided in this previous work. The proposed methodology was tested against few fire tests carried out across smaller beds (in the range of 1.1-1.5 m long) which did not allowed to achieve a fully steady state. In another preliminary study [17], a formulation for the evaluation of the fireline intensity, based on the mass burning rate, has been presented and tested against a few samples of data since few runs where fully steady in the previous fire tests (due to the short length and the preparation of the bed of pine needles). In the present paper, a series of 14 experimental runs has been carried out across 2 m long beds in order to propose meaningful average quantities (rate of spread, rate of mass loss and heat fluxes emitted from the flames and heat release rate) for three different fuel loads. This work focuses on the validation, against a new set of experimental data, of alternative methods to assess the fireline intensity developed previously. Some characteristics of the combustion processes (combustion efficiency and effective heat of combustion) are also evaluated. The geometry of the flame front has been recorded using photographs from side and rear perspectives. An image processing method has been developed to determine the average properties of such a radiant panel. The heat fluxes were measured ahead of the approaching fire front. The radiant fractions were estimated from heat fluxes and HRR. Finally, a methodology is proposed to compute the convective fraction from gas temperature measurements.

2 Experiments

2.1 Experimental device

The fire spread experiments were conducted by using a 1 MW Large Scale Heat Release Rate apparatus (LSHR). Fire tests were performed on a 2 m long and 2 m wide combustion table located under a 3 m × 3 m hood with a 1 m^3/s extraction system (Fig. 1). Two thermocouples (48 cm spaced) recorded the temperature of the combustion gases in the exhaust smoke duct. The bench was located on a load cell (sampling rate 1 Hz and 1 g accuracy) in order to record the mass loss over time during the fire spread across a fuel bed. In order to filter the signal of the mass, a moving average over a 5 s period was first performed. The mass loss rate was then determined during the steady state from the filtered data using a least squares regression technique to find the line of the best fit. Needles of *Pinus pinaster* were distributed uniformly on the table in order to obtain homogenous fuel beds of 1 m width and 2m long that occupy only the central part of the table. Particular attention was paid to the preparation of the fuel bed. It should be notice that a steady state is more easily reached when the fire spreads across a homogeneous bed of fuel. To ensure the homogeneity of the bed, the mass of the fuel was evenly informally distributed in 8 quadrants. The accuracy of the distribution of the pine needles was checked, measuring the height of the bed in the quadrants. This method provides better results than distributing the total mass of the fuel material over the whole combustion bench. Different fuel loads were tested: 0.6, 0.9 and 1.2 kg/m^2 that correspond to fuel beds height of 3, 5 and 7 cm. At least four repetitions were carried out for each fuel load. The net heat of combustion, the surface to volume ratio and density of the particles were $\Delta H_{c,net}$ = 20411 kJ/kg, σ = 3057 /m and ρ = 511 kg/m^3 respectively. The net heat of combustion was derived from the gross heat of combustion measured in an oxygen bomb calorimeter following the standard AFNOR NF EN 14918. The surface to volume ratio and density were measured following the methodology proposed by Moro [18]. The needles were oven dried at 60 °C for 24 hours. The resulting moisture content was between 3-5%. To ensure fast and linear ignition, a small amount of alcohol and a flame torch were

used. The experiments were conducted without wind and slope. The rate of spread was deduced from position of the fire over time every 0.25 m. Eight points were obtained for each experiment and a least-squares regression was used to fit a straight line to the data points. Three heat flux gauges (Medtherm Corporation) were used to measure heat fluxes during the fire spread. These transducers were placed at the end of the experimental bench, in the centre of the bed (Fig. 1). All heat flux gauges were cooled with circulating water. The first one was a total gauge (GTW-10-32-485A) calibrated up to 100 kW/m^2. The two others were radiant gauges (64P-02-24T) calibrated up to 20 kW/m^2. The radiant heat flux transducers were equipped with a Sapphire window with a view angle of 150°C. The total heat flux gauge (TG) and a radiant heat flux gauge (RG1) were oriented towards the flame and located 0.20 m above the bed. The second radiant heat flux gauge (RG2) was located at the end of the combustion bench, at mid height of the fuel layer in order to measure radiation from the bed (Fig. 1). The uncertainty for flux measurements was 3%. The sampling frequency was 100 Hz.

The length and the height of the flame were determined from photographs taken by a camera operating in the visible spectrum located perpendicularly to the fire spread direction. The camera was automatically controlled to take pictures every 2 to 4 seconds, depending on the rate of spread of the fire. For each experience, from 30 to 50 images were analyzed to compute the length and the height of the flame front. Fig. 2 shows how these variables were measured since, as pointed out by Anderson [19], flame geometry descriptors are not univocally described on the literature. Flame length and flame height were expressed following these suggestions. Images were processed using Matlab®. A checkerboard was used to determine the correspondence between the coordinates of a point in the image and in the real world, assuming that the camera obeyed a linear projection model. Then, a graphical interface allowed user selecting the position of the base and the tip of the flame for each image. These data were automatically processed to obtain the flame length and flame height.

2.2 Calorimetric calculation

The heat release rate (HRR) is among the most important parameter for understanding combustion processes [20] but it has rarely been investigated for spreading fires across forest fuels [16-17]. This quantity cannot be a-priori estimated from the fundamental properties of the fuel material and experiments need to be carried out to determine it. The measurement of the HRR was determined from gas volume fractions and mass flow rate of exhausted gas following the formulation derived by Parker [21]. When estimating the HRR of a reaction from the chemical species concentration, the main hypothesis lays in the knowledge of the evolution of the combustion gases during the reaction. The combustion of pine needles was represented by the stoichiometric reaction for the complete combustion of lignocellulosic materials, given by [22]:

$$C_{4.15}H_{6.65}O_{2.51} + 4.56\left(O_2 + 3.76N_2\right) \rightarrow 4.15CO_2 + \frac{6.65}{2}H_2O + 17.14N_2 \quad (1)$$

The calculations were performed by using simplifying assumptions; the main ones are listed below. The amount of energy released by complete combustion per unit mass of oxygen consumed is taken constant. All gases are considered to behave as ideal gases. The analyzed air is defined by its composition in O_2, CO_2, H_2O and N_2. All other gases are lumped into N_2. The heat release rate is computed assuming a constant amount of energy released per unit mass of oxygen consumed:

$$HRR = E\left(\dot{n}_{O_2}^{\circ} - \dot{n}_{O_2}\right)W_{O_2} \quad (2)$$

The detailed calculation is provided in [17]. The HRR is given by the three following relations:

$$HRR = \frac{E\rho_0 W_{O_2}}{W_{air}}\left(1 - X_{H_2O}^{\circ}\right)X_{O_2}^{a^{\circ}}\dot{V}_{s,298}\left[\frac{\phi}{(1-\phi)+\alpha.\phi}\right] \quad (3)$$

$$\dot{V}_{s,298} = 22.4A\frac{k_t}{k_p}\sqrt{\frac{\Delta P}{T_S}} \quad (4)$$

$$\phi = \frac{X_{O_2}^{a^\circ}\left(1 - X_{CO_2}^{a}\right) - X_{O_2}^{a}\left(1 - X_{CO_2}^{a^\circ}\right)}{X_{O_2}^{a^\circ}\left(1 - X_{CO_2}^{a} - X_{O_2}^{a}\right)} \quad (5)$$

2.3 Uncertainty of HRR measurement from LSHR

The HRR is computed from many variables and each variable has a corresponding uncertainty, which is reflected in the mathematical function giving the HRR. In addition to the uncertainties pertaining to random variable and those based on scientific judgment or specifications [23], for large scale apparatus, one can also mention random effects on fire growth that can affect the repeatability of the tests [24] and increase the uncertainty. The LSHR used in this study was installed by Fire Testing Technology Ltd (FTT). The instrumentation packages supplied are those corresponding to the Room Corner Test [25] for which Axelsson et al. [26] have analyzed the uncertainty considering individual sources of errors for rate of heat release measurements. The combined expanded uncertainty was provided with a coverage factor of 2, giving a confidence level of 95%. Uncertainty of ±10.6% at 150 kW level was reported in that study. The uncertainties of the oxygen concentration measurement, followed by the heat of combustion and the mass flow rate measurement were identified as the major sources of uncertainty. To reduce the measurement uncertainties, analyzers were developed specifically for FTT Calorimeters, incorporating an enhanced Servomex 4100 featuring a high stability temperature controlled paramagnetic oxygen sensor with flow control and by-pass for fast response. The accuracy of the exhaust duct volume flow measurement was also improved by calibrating the bi-directional probes in a controlled flow. In our case, the combined expanded uncertainty was decreased to ±3.6% due to the attention paid to O_2 analysers and estimation of E. The variation in HRRs due to the variation in E is given is provided in [17]. When the composition of the fuel is known, a more accurate value for E can be determined. Following the assumption of the stoichiometric reaction given in eq. (1) (valid since the experiments were conducted under well-ventilated conditions), the OCC energy constants can be estimated from the fuels ultimate analysis and low heat of combustion:

$$E_{st}^{fuel} = \frac{\Delta H_{c,net}^{fuel} . W_{fuel}}{4.65 . W_{O_2}} \quad (6)$$

The estimated energy constant is then equal to 13.98 MJ/kg that corresponds to an increase of 6.7 % compared to Huggett's constant (13.1 MJ/kg). It should be notice that the use of the Huggett's constant would therefore underestimate the HRR calculations.

3 Results and discussion

3.1 Fire behaviour and properties

Spreading fires exhibited flame fronts with nearly linear shape. A weak curvature could appear at the edge of the bed of fuel resulting in a lower height of the flame height in this region. However, the length of the flame front was assumed to be equal to the length of the fuel bed. The measurements of the fire properties for the whole set of experiments are reported in Table 1. The fuel consumption ratio was very high (>95%) since the fuel was composed of pine needles with fine diameters. The average values of flame heights were 24.3, 41.6 and 57.3 cm for the 0.6, 0.9 and 1.2 kg/m² fuel load, respectively. For the flame lengths, we obtained 25.5, 44.4 and 60.2 cm. The values of the flame length and height were close because the flames had a low inclination and slightly leaned backwards. The mean values increased by a factor of 1.7 and 2.4 with increasing the fuel load by a factor of 1.5 and 2. The positions of the fire versus time are plotted in Fig. 3 for 0.6 and 1.2 kg/m² fuel load. The fires reached a quasi-steady state (R^2>0.99). The repeatability of the experiments was generally very satisfactory except for fire tests n° 09_3 and 12_2 which were conducted under abnormally high air moisture content (>65%) compared to the other experiments. Consequently the fire travelled more slowly for these two last runs. These two fire tests were excluded from the final analysis. The average rates of spread were 3.7, 5.0 and 6.3 mm/s for the 0.6, 0.9 and 1.2 kg/m² fuel load, respectively. The mean values increased by a factor of 1.35 and 1.70 with increasing the fuel load by a factor of 1.5 and 2.

The temporal evolution of the mass of the fuel bed is superimposed in Fig. 3. The average mass loss rates (Table 1) were 2.2, 5.3 and 8.1 g/s for the 0.6, 0.9 and 1.2 kg/m² fuel load, respectively. The mean values increased by a factor of 2.20 and 3.59 with increasing the fuel load by a factor of 1.5 and 2. These values are representative of the whole thermal degradation process of the pine needles, namely pyrolysis and char oxidation. Since the needles were oven dried before the tests, the mass loss due to dehydration was not significant.

The burning behaviour of the solid fuel influenced the heat released during fire spread. The instantaneous heat release rate and mass loss rate during the fire tests are displayed in Fig. 4 for 0.6 and 1.2 kg/m². The similarity of the curves highlights a close relationship between these two different quantities. Indeed, the rate of heat released is directly proportional to the mass loss rate and proportionality constant is defined as the heat of combustion. This aspect will be detailed in a later section of the paper. Nevertheless, it should be noticed that the accuracy of the load cell did not allowed computing the mass loss at the end of the tests where the remaining mass is very small. This explains the discrepancies between the two curves after the flameout. The greater the fuel load, the greater the heat release rate. The flameout occurred earlier for higher fuel load due to the increase in the rate of spread. The average HRR were computed during the quasi-steady state (Table 1). The average heat release rates were 41, 92 and 155 kW for the 0.6 to 0.9 and 1.2 kg/m² fuel load, respectively. The mean values increased by a factor of 2.13 and 3.63 with increasing the fuel load by a factor of 1.5 and 2. These values are close to the ones obtained for the mass loss rate, which indicates a linear relation between HRR and mass loss rate. The total heat released (THR) was obtained by integration of the HRR curves during the whole experiment (Table 1). The average total heat released were 21, 33 and 41 MJ for the 0.6 to 0.9 and 1.2 kg/m² fuel load, respectively. The total heat released depends also linearly on the load.

The burning rate is defined as the mass rate of fuel consumed by the chemical reaction. As proposed by Quintiere [27] for solids, the mean mass loss rate of the fuel was used to estimate the burning rate. The fireline intensity (kW/m) corresponds to the ratio between the HRR obtained by OCC and the

length of the fire perimeter. The burning rates per unit length versus the fireline intensity for the whole set of experiments are plotted in Fig. 5. The higher the fireline intensity, the greater the burning rate. Indeed, results exhibit a linear relationship with a very good correlation coefficient (R^2>0.99). The fireline intensity can be obtained from the product of the mass loss per unit length (kg/s/m) by an effective heat of combustion of about 18 556 kJ/kg. This value was evaluated from the slope of the curve represented in Fig. 5. It should be noticed that the effective heat of combustion is lower than the net heat of combustion of *Pinus pinaster* needles (20 411 kJ/kg). This highlights that a correction of the heat yield introducing the combustion efficiency [27] is required and its estimation is provided in the following section.

3.2 Effective heat of combustion

The effective heat of combustion H_{eff} is representative for real fire conditions where there is unlimited availability of air. A global (smoldering and flaming) effective heat of combustion was determined for each test, i, by dividing the total heat released by the total mass lost during the quasi-steady stage:

$$H_{eff}^{i} = \int_{T_{in}}^{T_{fi}} HRR\,dt \Big/ \left(m_{in} - m_{fi}\right) \tag{7}$$

where subscript in and superscript fi are for initial and final time of steady stage. Then, for each fuel load, a mean effective heat of combustion was calculated by averaging the global effective heat of combustion obtained for the set of N tests:

$$\overline{H_{eff}^{i}} = \frac{1}{N}\sum_{i=1}^{N} H_{eff}^{i} \tag{8}$$

The combustion efficiency represents the ratio between the average effective heat of combustion $\overline{H_{eff}^{i}}$ and the heat yield:

$$\chi_{eff} = \overline{H_{eff}^{i}} \Big/ H \tag{9}$$

H is calculated from the net heat of combustion adapted to the moisture content of fuel:

$$H = \frac{\Delta H_{c,net}}{1 + p_m / 100} \tag{10}$$

Both mean effective heat of combustion and combustion efficiency are provided in Table 2 for all fuel loads. The effective heat of combustion and the combustion efficiency scarcely varied for the fuel loads studied. The mean value of effective heat of combustion is 18227 kJ/kg. This value corresponds to combustion efficiency equal to 0.937. These values are close to those found previously and are consistent with the measurements of Babrauskas [28] for flaming combustion of Douglas-fir. In a free burn test, the fuel is burned with unlimited access to air, but some of the volatiles do not burn completely, leaving for example CO, soot and unburnt hydrocarbons, containing further potential energy.

3.3 Alternative estimations for the fireline intensity

Consideration of the previously defined combustion efficiency leads to modify the Byram's relationship as follow:

$$I_{MBF} = w \chi_{eff} H_{comb} r \tag{11}$$

The results of the comparison of the fireline intensities predicted by the modified Byram formulation (MBF) and measured by oxygen consumption are plotted in Fig. 6. The agreement is very satisfying when the combustion efficiency is introduced. The few discrepancies (about 2%) were mainly due to the errors in the measurement of the mass consumed in the flaming zone. The uncertainties in the measurement of r were reduced since average values were used. The mass loss was estimated for the

whole duration of the experiments, between ignition and extinction of embers, which potentially overestimates the mass consumed in the combustion area.

As seen previously (Fig 5), the fireline intensity can also be obtained from the mass loss rate approach (MLR):

$$I_{MLR} = \dot{m}' \chi_{eff} H \tag{12}$$

The results of the comparison of the fireline intensities obtained from the mass loss rate approach and measured by oxygen consumption are superimposed in Fig. 6. This formulation also exhibits a very good agreement for this set of experiments. In the laboratory, most of the test conditions are controlled and the fire properties can be measured with relatively low uncertainties which allow academic case studies. In quasi-steady-state conditions, where the rate of spread is constant and fire front linear, establishing a mass balance over the fire front allows estimating the rate of burning per unit length of fire front by the product of the mass of the fuel consumed per unit area and the rate of spread (Fig. 7). That kind of relation was used by Byram [1] and Rothermel [29] to derive their formulation. This approximation may not be very accurate in the field since fire front is rarely linear in actual fires and furthermore the measurement of the last two quantities has uncertainties. In particular, the determination of the load of the consumed fuel in the flaming region of a wildfire is very difficult since vegetation is composed by particles of different size class (leaves, needles, branches and trunk). Only the particles with diameter lower than 6 mm (1 hour fuel) participates in the spread of the fire. The thermal degradation of the material with diameter greater than 2 cm, which does not participate in fire spread, occurs at the end of the active flaming region. Thus, the mass loss in the flaming region cannot be determined from fuel consumption efficiency using post-fire measurements of the remaining chars. Although OCC is not appropriate at field scale to investigate the intensity of fires spreading in the open, the burning rate formulation seems promising, provided mass loss rate per unit length of fire front (of the finest fuel particles) can be measured at that scale.

3.4 Heat fluxes

The time evolution of the total and radiant heat fluxes emitted by the flame during the fire spread is shown in Fig. 8 for two fuel loads (0.6 and 1.2 kg/m^2). The position of the 3 gauges (TG, RG1 and RG2) is indicated in Fig 1. In the preheating zone, the heat fluxes progressively increased up to maximum values which varied according to the fuel loads (between 7 and 15 kW/m²). This maximum corresponds to the moment when the flame was at the end of the bench, i.e. at the closest point of the measurement device. As the total and radiant heat fluxes coincided in the preheating zone, heat transfer was mainly due to radiation. In the flame zone, a greater difference appeared between both signals. This is characteristic of heat transfers combining radiation and convection. To investigate the radiation emitted by the embers, the measurements obtained with RG2 were used (Fig. 8). The radiant heat flux measured by RG2 remained low until the flame front was close to the sensor. Thus, this heat flux gauge did not record the radiation emitted by the flame. This was due to the view angle of the sensor but also to the absorption of needles that prevents flame radiation reaching the sensor. When the flame front reached the end of the bench, the heat flux measured by RG2 increased. The maximum of the curve appeared, however, after the extinction of the flame. Thus, the radiant heat flux measured by this sensor after the flame extinction corresponded only to radiation from the embers. The maximum heat flux recorded for embers was higher than that of the flame. This was due to the fact that the net calorific value of the coal was higher than that of the pyrolysis gases.

From the measurements recorded by the two radiant heat flux gauges, the radiant fractions emitted by the flame and by the embers were calculated. The radiant fraction corresponds to the ratio between the radiative heat release rate and the total heat release rate (HRR).

$$\chi_{rad} = \frac{HRR_{rad}}{HRR} \tag{13}$$

For the flame, the radiative heat release rate can be calculated from the measurements performed with the radiant heat flux gauge q_{RG1} (Fig. 8) by considering the view factor (F) and the emission surface of the flame front (S):

$$q_{RG1} = \frac{HRR_{rad}}{S}.F \tag{14}$$

The emission surface S was taken equal to 2 x 1x H. The factor 2 appeared in this expression because both sides of the flame were considered for radiant emission. The flame front emitted indeed ahead of the fire front and towards the rear of the fire spread.

Therefore, by combining Eq. 13 and 14, the radiant fraction of the flame $\chi_{rad,flame}$ corresponds to:

$$\chi_{rad,flame} = \frac{q_{RG1}.S}{HRR.F} \tag{15}$$

By using a solid-flame model, the view factor between the flame and the radiant heat flux gauge was determined with the following assumptions (Fig. 9): (i) the radiant heat flux gauge was a differential planar element; (ii) the radiant heat flux gauge passed through a corner and was at a distance D of the flame front calculated from the flame position (Fig. 3); (iii) the flame was considered vertical due to the low inclination and (iv) the flame was modelled by four finite parallel rectangles with a length equal to A=0.5 m. The height of the lower rectangles was taken equal to B_1=B_2=0.2 m. The height of the top rectangles was equal to B_3=B_4=H-B_1, where H is the flame height (Table 1). Therefore, the view factor for each rectangle *i* is given by [30]:

$$F_i = \frac{1}{2\pi}\left(\frac{X}{\left(1+X^2\right)^{1/2}} \tan^{-1}\left[\frac{Y}{\left(1+X^2\right)^{1/2}} \right] + \frac{Y}{\left(1+Y^2\right)^{1/2}} \tan^{-1}\left[\frac{X}{\left(1+Y^2\right)^{1/2}} \right] \right) \tag{16}$$

where X=A/D and Y=B_i/D (Fig. 9).

Thus, the radiant fraction of the flame is equal to:

$$\chi_{rad,flame} = \frac{q_{RG1}.S}{HRR.\sum_i F_i} \quad (17)$$

As for the flame, the radiative heat release rate of the embers can be calculated from the measurements performed with the radiant heat flux gauge q_{RG2} by considering the view factor and the emission surface of the embers. Therefore, the radiant fraction of the flame $\chi_{rad,embers}$ was given by:

$$\chi_{rad,embers} = \frac{q_{RG2}.S_{embers}}{HRR.\sum_i F_i} \quad (18)$$

where S_{embers} is the emission surface of the embers.

The view factor between the embers and the radiant heat flux gauge was calculated in the same way as the flame. Assumptions (i) and (ii) were kept. The embers were modelled by a rectangular parallelepiped having a width of 1 m, a height corresponding to the fuel bed and a depth varying according to the experiences (Fig. 9). Only the maximal radiant heat fluxes measured by the heat flux gauge RG2 (q_{RG2}) were used. The distance between the radiant heat flux gauge and the embers was equal to 1 cm.

Table 2 shows the mean radiant fractions for the flame and the embers. The radiant fraction emitted by the flame decreased slightly with increasing fuel loads (between 0.101 and 0.091). For the embers, the radiant fraction increased with the fuel loads (between 0.073 and 0.133). This was likely due to the increase of the ember volume. The radiant fraction of the embers is more affected by the fuel load than that of the flame. This is due to the position of the flame, which is oriented slightly backwards. Only a small part of the flame contributes to radiative heat transfers towards the solid fuel. These results are only valid in the case of a fire spread without slope and without wind. By adding the contribution of the flame and embers, the overall radiant fraction was equal to 17.4, 19.9 and 22.4% respectively for 0.6, 0.9 and 1.2 kg/m^2. These values are in agreement with those found in literature [15].

The convective heat release HRR_{conv} was calculated with [31]:

$$HRR_{conv} = \dot{M}_{mix} \cdot \int_{T_a}^{T_g} c_{p,mix}(T).dT \tag{19}$$

The mass flow rate of the chemical compounds-air mixture is determined from the volumetric flow rate of the mixture through the duct. The density and the specific heat of the mixture were taken equal to those of dry air. The gas temperature was calculated from the measurements recorded by the thermocouples TK1 and TK2 placed in the gas measuring section (Fig. 1) by considering the heat losses in the duct before the measurement station. For a duct section with a length dx, the heat balance during the quasi-steady state is represented by:

$$\dot{M}_{mix}.c_{p,mix}T(x) = \dot{M}_{mix}.c_{p,mix}T(x+dx) + \Phi_{loss} \tag{20}$$

The heat losses were modelled by:

$$\Phi_{loss} = \pi.d.dx.U.(T - T_a) \tag{21}$$

By combining eq. (20)-(21), one obtains:

$$\frac{dT(x)}{dx} + aT(x) = aT_a \tag{22}$$

with $a = \dfrac{\pi.d.U}{\dot{M}_{mix}.c_{p,mix}}$

The temperature in the duct is therefore given by:

$$T(x) = T_a + (T_{TK2} - T_a).e^{a.(x_2 - x)} \tag{23}$$

Where T_{TK2} is the temperature measured by thermocouple TK2 and x_2 correspond to the distance between the beginning of the duct and this thermocouple (x_2=5.576 m). The value of A can be estimated by using the measurement of TK1 and TK2:

$$A = \frac{1}{x_2 - x_1} \ln \frac{T_{TK1} - T_a}{T_{TK2} - T_a} \quad (24)$$

Where T_{TK1} is the temperature measured by thermocouple TK1, x_1 correspond to the distance between the beginning of the duct and this thermocouple (x_1=6.056 m). Finally, the gas temperature at duct entry was obtained by combining eq. (23)-(24) with x=0:

$$T_g = T_a + \left[\frac{\left(T_{TK1} - T_a\right)^{x_2}}{\left(T_{TK2} - T_a\right)^{x_1}} \right]^{\frac{1}{x_2 - x_1}} \quad (25)$$

The convective fraction was then calculated with:

$$\chi_{conv} = \frac{HRR_{conv}}{HRR} \quad (26)$$

The mean convective fractions calculated on the quasi-steady state are given in Table 2. The convective fractions were equal to 0.838, 0.802 and 0.685, respectively for 0.6, 0.9 and 1.2 kg/m^2. The convective fraction decreased when the fuel load increased, what corresponds to an increase of the radiant fraction. The sum of the radiant and convective fractions was 1.011, 1.001 and 0.910, respectively for 0.6, 0.9 and 1.2 kg/m^2. In this study, both fractions were calculated separately for each fire test. The standard deviations for each fuel load are provided in the Table 2. Taking into account these deviations shows that the sum can be considered equal to unity. It should be noticed that the determination of the radiative and convective fractions for each test is subject to uncertainties since the variables (HRR, view factor, flame or ember surface, heat transmission coefficient, temperature) from which they are estimated encompass uncertainties. For the fuel load of 0.6 kg/m², the sum of the average fractions is very close to 1. For 1.2 kg/m^2, the convective fraction was likely underestimated. During propagation with this fuel load, the suction flow of the hood was not sufficient to evacuate the gases emitted by the fire. A layer of smoke appeared above the hood, what increased heat losses in the device. The gas temperature calculated from the eq. (25) was thus underestimated, leading to an underestimation of HRR_{conv} for a fuel load of 1.2 kg/m^2.

Conclusion

In this study, oxygen consumption calorimetry was used to analyze the spreading of fire across pine needles beds under no slope and no wind conditions. This technique coupled with heat flux gauges provided measurements of HRR, fireline intensity and heat fluxes. From these data, some global properties of the fire such as the combustion efficiency or the radiant and convective fractions were calculated for three different fuel loads. These results are of crucial importance for modellers that have to deal with little information available on the source terms (HRR, radiative and convective fractions) useful for forest fire modelling. The main results of this work can be summarized as follows:

- The HRR, the burning rate and the rate of spread increased with the fuel load.
- The effective heat of combustion varied scarcely for the fuel loads studied (about 18 227 kJ/kg), leading to combustion efficiency of 0.937.
- The fireline intensity can be accurately estimated either with the mass loss rate approach or with the Byram's formulation when combustion efficiency is considered for steady state fires.
- The radiant fraction emitted by the flame was around 9.7 % and decreases with increasing fuel loads. For the embers, the radiant fraction increases with the fuel load. The global radiant fraction was in the range of 17.4 – 22.4 %. The convective heat release rate was also calculated. The convective fraction decreases as the fuel load increases.

References

[1] G.M. Byram, in: K.P. Davis (Ed.), Forest fire: control and use, Mc Graw-Hill, New York, 1959, p 61

[2] M.E. Alexander, M.G. Cruz, Modelling the effects of surface and crown fire behaviour on serotinous cone opening in jack pine and lodgepole pine forests,Int. J. Wildland Fire 21 (2012) 95-113.

[3] M.E. Alexander, Calculating and interpreting forest fire intensities, Can. J. Bot. 60 (1982) 349-357.

[4] R.M. Nelson, C.W. Adkins, Flame characteristics of wind-driven surface fires, Can. J. For. Res. 16 (1986) 1293–1300.

[5] P.A. Santoni, A. Simeoni, J.L. Rossi, F. Bosseur, F. Morandini, X. Silvani, J.H. Balbi, D. Cancellieri Et L. Rossi, Instrumentation of wildland fire: characterisation of a fire spreading through Mediterranean shrub, Fire Safety J. 4l (2006), 171-184.

[6] T. Ohlemiller, D. Corley, Heat Release Rate and Induced Wind Field in a Large Scale Fire, Combust. Sci. and Tech. 97 (1994) 315–330.

[7] B W Butler, J Cohen, D J Latham, R D Schuette, P Sopko, K S Shannon, D Jimenez, L S Bradshaw, Measurements of radiant emissive power and temperatures in crown fires, Can. J. Forest Res. 36 (2004) 1577-1587.

[8] F. Morandini, X. Silvani, L. Rossi, P.A. Santoni, A. Simeoni, J.H. Balbi, J. L Rossi, T. Marcelli, Fire spread experiment across Mediterranean shrub: influence of wind on flame front properties, Fire Safety J. 41 (2006) 229–235.

[9] X. Silvani, F. Morandini, Fire spread experiments in the field: Temperature and heat fluxes measurements, Fire Safety J. 44 (2009) 279-285.

[10] F. Morandini, X. Silvani, Experimental investigation of the physical mechanisms governing the spread of wildfires. In. J. Wildland Fire 19 (2010) 570-582.

[11] J.L. Dupuy, J. Maréchal, Slope effect on laboratory fire spread: contribution of radiation and convection to fuel bed preheating, Int. J. Wildland Fire 20 (2011) 289–307.

[12] I Knight, M Dando, Radiation above bushfires: Report to State Electricity Commission of Victoria and Electricity Trust of South Australia. National Bushfire Research Unit, CSIRO, Canberra, 1989.

[13] P.H. Freeborn, M.J. Wooster, W.M. Hao, C.A. Ryan, B.L. Nordgren, S.P. Baker, C. Ichoku, Relationships between energy release, fuel mass loss and trace gas and aerosol emissions during laboratory biomass fires. J. Geophys. Res. 113 (2008) D01301

[14] R. L. Kremens, M. B. Dickinson, A. S. Bova, Radiant flux density, energy density and fuel consumption in mixed-oak forest surface fires, Int. J. Wildland Fire 21 (2012) 722–730.

[15] A. Tewarson, Generation of Heat and Chemical Compounds in Fires. SFPE Handbook of Fire Protection Engineering, National Fire Protection Association, 2002.

[16] P.A. Santoni, F. Morandini, T. Barboni, Determination of fireline intensity by oxygen consumption calorimetry, J. Therm. Anal. Calorim. 104, 3 (2011) 1005-1015.

[17] P.A. Santoni, F. Morandini, T. Barboni, Steady and unsteady fireline intensity of spreading fires at laboratory scale, Open Thermodyn. J. 4 (2010) 212-219.

[18] C. Moro, Détermination des caractéristiques physiques de particules de quelques espèces forestières méditerranéennes, INRA PIF2006-06, 2006.

[19] Anderson W, Pastor E, Butler B, Catchpole E, Dupuy JL, Fernandes P, Guijarro M, Mendes-Lopes JM, Ventura J, Evaluating models to estimate flame characteristics for free-burning fires using laboratory and field data, *Proc 5th International Conference on Forest Fire Research (Figueria da Foz, Portugal, 27-30 November 2006).*

[20] V. Babrauskas, R.D. Peacock, Heat Release Rate: The Single Most Important Variable in Fire Hazard, Fire Safety J. 18 (1992) 255–292.

[21] W.J. Parker, Calculations of the heat release rate by oxygen consumption for various applications. NBSIR 81–2427–1, 1982.

[22] H. Biteau, T. Steinhaus, C. Schemel, A. Simeoni, G. Marlair, N. Bal, J.L. Torero, Calculation methods for the heat release rate of materials of unknown composition, *Proc. 9th IAFSS International Symposium on Fire Safety Science (Karlsruhe, Germany, 21-26 September 2008*

[23] R.A. Bryant, G.W. Mulholland, A guide to characterizing heat release rate measurement uncertainty for full-scale fire tests, Fire Mater, 32 (2008) 121–39.

[24] M.L. Janssens, Measurement needs for fire safety proceedings, Proceedings of an International workshop. NISTIR 6527, 2000, 186–200.

[25] International Standard. Fire tests—full scale room test for surface products, ISO 9705. Geneva: International Organization for Standardization; 1993.

[26] J. Axelsson, P. Andersson, A. Lönnermark, P. Van Hees, I. Wetterlund, Uncertainties in measuring heat and smoke release rates in the Room/Corner test and the SBI, SP report 2001:04, Boras: Swedish National Testing and Research Institute, 2001.

[27] J. Quintiere, Fundamentals of fire phenomena. John Wiley & Sons Ltd., 2006 p. 227–286.

[28] V. Babrauskas, in: M.A. Quincy, J.P. Di Nenno, W.D. Walton (Eds), Heat Release Rates, The SFPE Handbook of Fire Protection Engineering, National Fire Protection Association and The Society of Fire Protection Engineers, 2002, p 1–37.

[29] R.C. Rothermel A mathematical model for predicting fire spread in wildland fuels. Res. Pap. INT-115. Ogden, UT: U.S. Department of Agriculture, Intermountain Forest and Range Experiment Station. 40 p.

[30] H.C. Hottel, Radiant heat transmission between surfaces separated by non-absorbing media, Trans. ASME, vol. 53, FSP-53-196, (1931) 265-273.

[31] M. Dahlberg, Error analysis for heat release measurements with the SP Industry Calorimeter, SP Report 1994:29, Swedish National Testing and Research Institute, Borås, 1994.

Table 1. Properties of the fire spread experiments.

Test n°	Fuel load (kg/m^2)	Flame height (standard deviation) (cm)	Flame length (standard deviation) (cm)	ROS (mm/s)	MLR (g/s)	Mean HRR (kW)	Peak HRR (kW)	THR (MJ)	Peak Radiant (Total) Heat Fluxes from flame (kW/m^2)
06_1	0.6	24.2 (5.4)	25.3 (5.2)	3.5	2.2	41.5	58.4	20.4	6.9 (8.1)
06_2	0.6	26.9 (7.3)	28.9 (7.2)	3.8	2.4	43.9	59.73	20.9	6.5 (8.2)
06_4	0.6	26.3 (4.7)	27.1 (4.6)	4.0	2.3	44.9	61.1	21.1	6.0 (7.3)
06_5	0.6	23.3 (5.9)	24.0 (5.8)	3.5	2.1	40.1	57.9	20.6	6.1 (7.4)
06_6	0.6	20.7 (5.0)	22.2 (4.6)	3.8	2.2	44.4	57.2	21.8	5.6 (7.0)
09_1	0.9	49.2 (7.7)	52.1 (8.1)	5.0	5.3	89.7	114.7	32.7	9.9 (11.7)
09_2	0.9	48.9 (7.2)	53.3 (8.2)	5.3	5.7	97.8	123.8	33.9	8.6 (10.4)
09_3	0.9	24.6 (6.1)	27.3 (5.9)	3.3	2.8	50.8	67.1	29.0	5.4 (6.9)
09_4	0.9	40.2 (7.8)	43.7 (8.3)	4.9	4.8	87.3	107.7	33.3	9.4 (11.1)
09_5	0.9	44.9 (6.9)	45.4 (6.9)	4.9	5.4	91.4	120.8	33.9	9.1 (11.0)
12_1	1.2	64.4 (10.1)	67.5 (12.1)	5.9	7.9	147.7	175.2	41.3	12.1 (14.8)
12_2	1.2	32.5 (7.3)	35.7 (7.1)	3.5	4.0	69.9	93.7	36.2	6.2 (7.9)
12_3	1.2	59.3 (13.2)	61.8 (13.2)	5.8	7.6	144.0	163.5	39.9	12.8 (15.6)
12_4	1.2	72.9 (12.3)	75.6 (12.4)	7.3	8.9	171.3	200.4	45.6	14.0 (17.1)

Table 2. Average values (standard deviations) of the effective heat of combustion, combustion efficiency, radiant and convective fractions for the three fuel loads

Fuel load (kg/m^2)	H_{eff} (kJ/kg)	χ_{eff}	$\chi_{rad,flame}$	$\chi_{rad,embers}$	χ_{conv}
0.6	18008 (415)	0.926 (0.021)	0.101 (0.008)	0.073 (0.019)	0.838 (0.019)
0.9	18586 (730)	0.956 (0.039)	0.099 (0.010)	0.099 (0.018)	0.802 (0.052)
1.2	18086 (563)	0.931 (0.028)	0.091 (0.002)	0.133 (0.022)	0.685 (0.077)

Figures

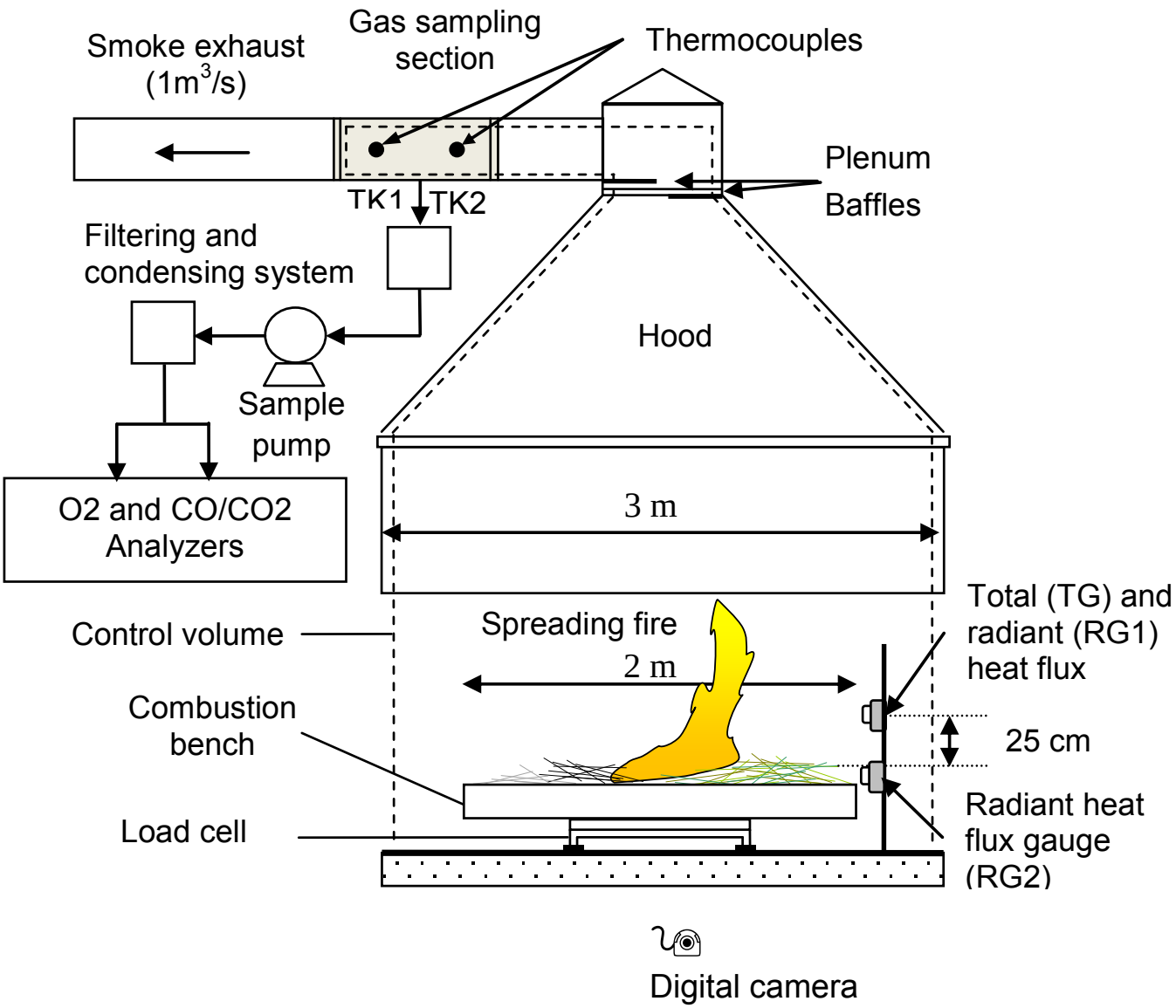

Fig. 1: Experimental device used for fire tests: Large Scale Heat Release apparatus, combustion table, load cell and heat flux gauges

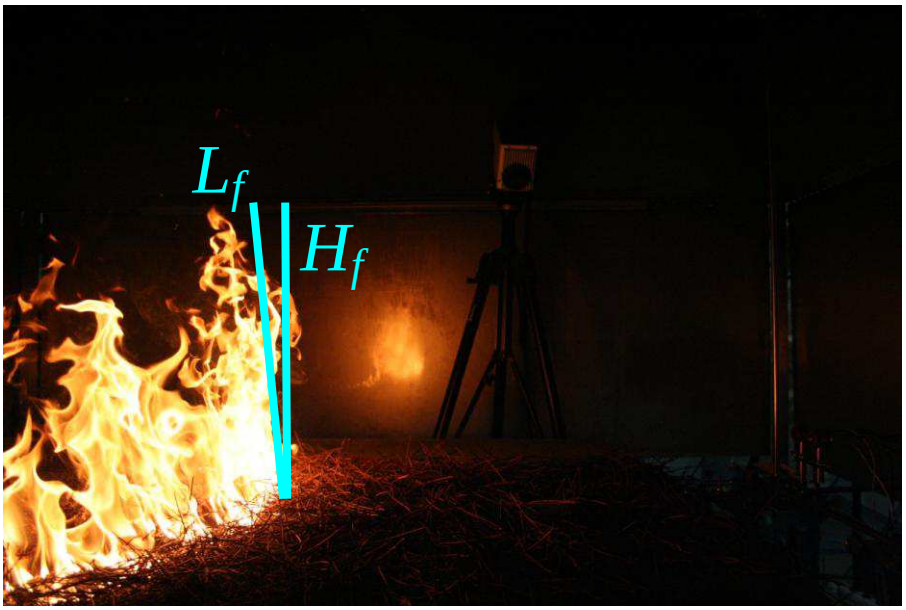

Fig. 2: Geometric descriptors of the flame front

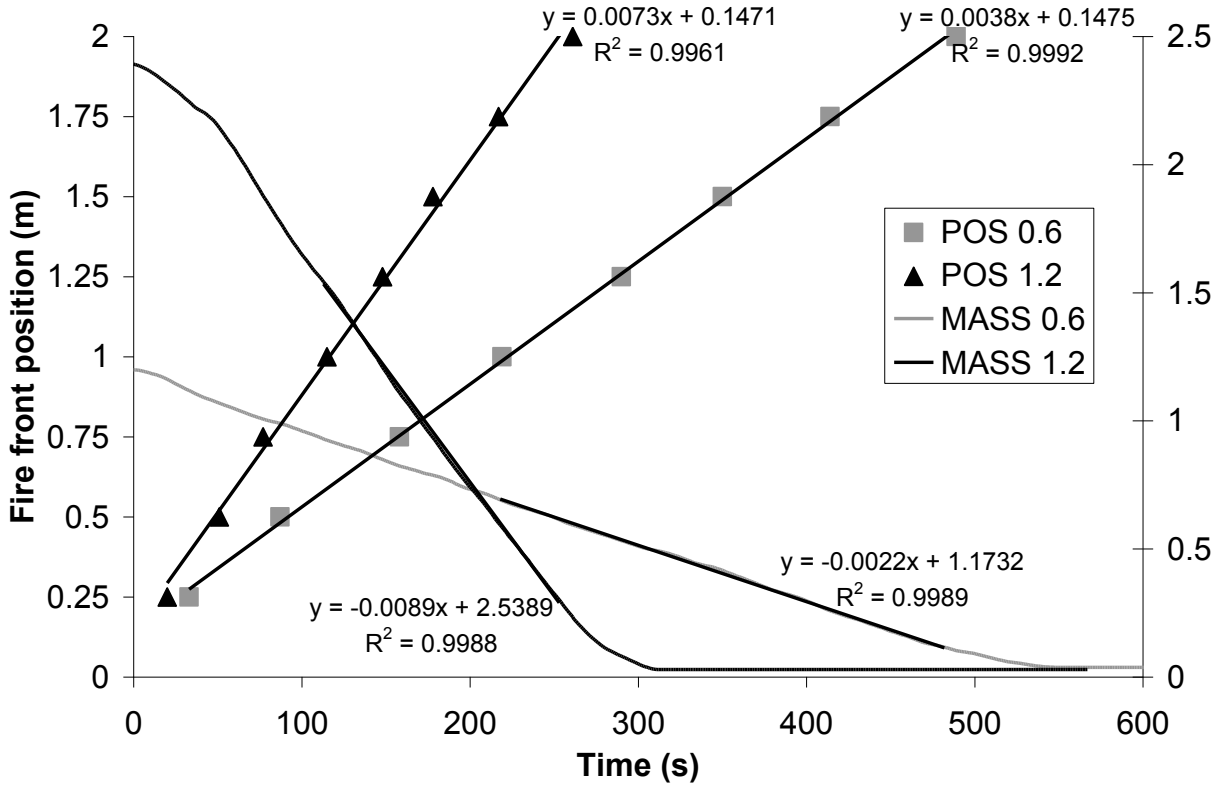

Fig. 3: Fire front position and measurements of the mass versus time for 0.6 and 1.2 kg/m²

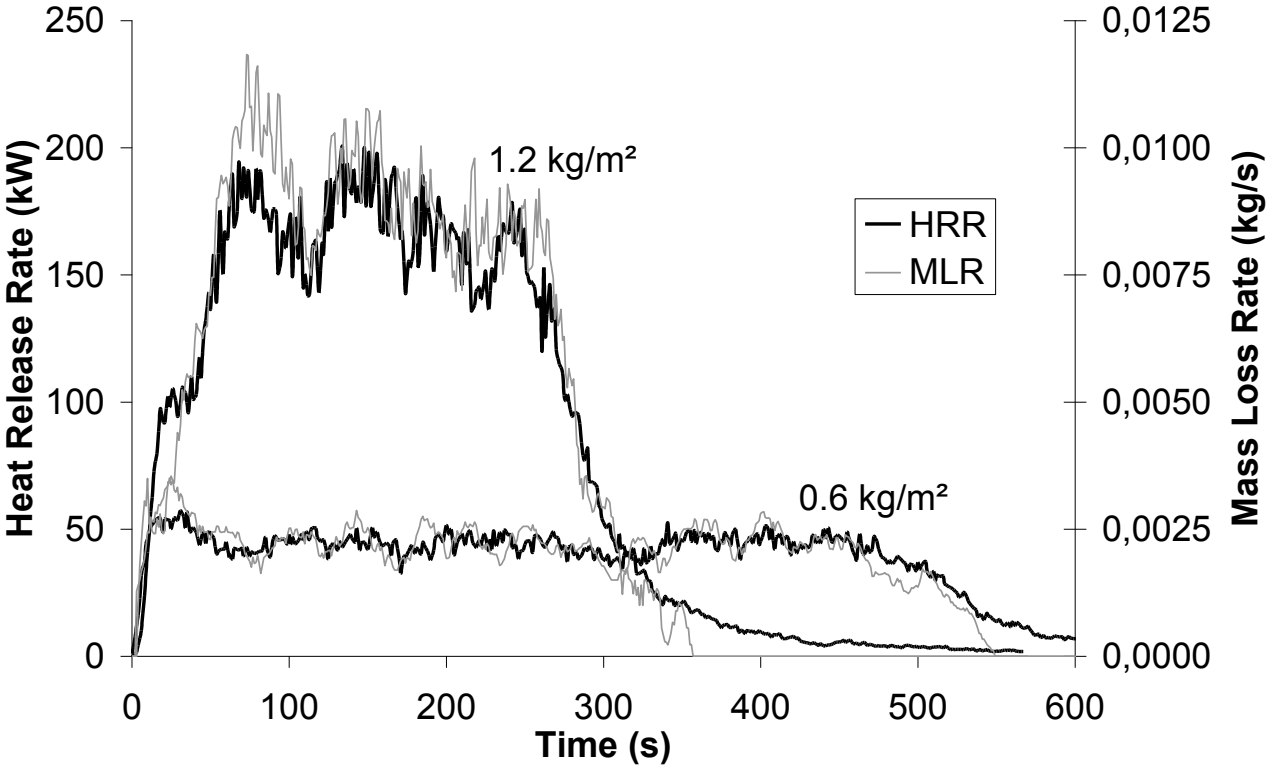

Fig. 4: Heat release rate and mass loss rate versus time for 0.6 and 1.2 kg/m²

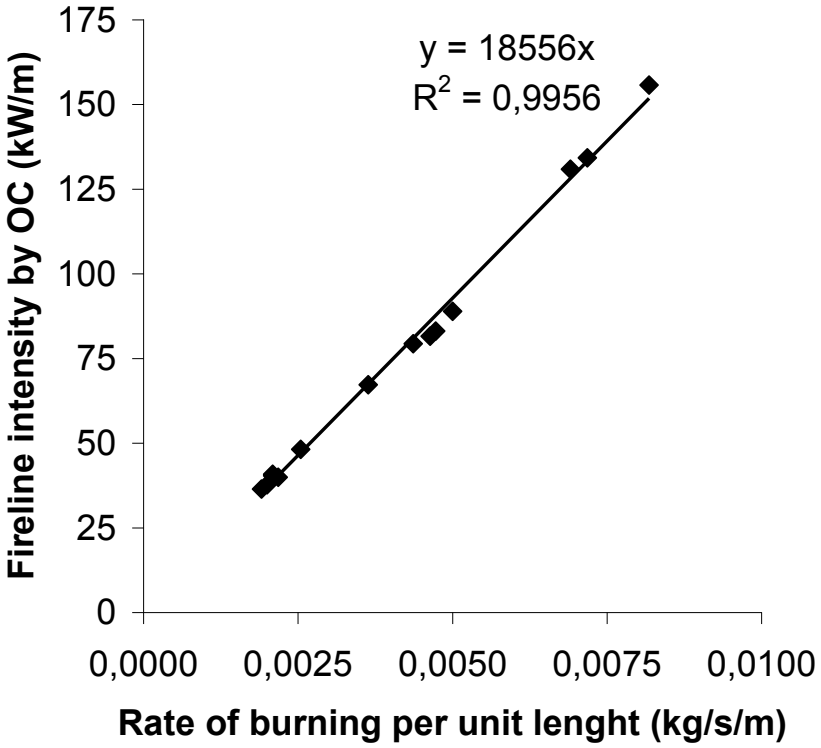

Fig. 5: Fireline intensity versus rate of burning per unit length

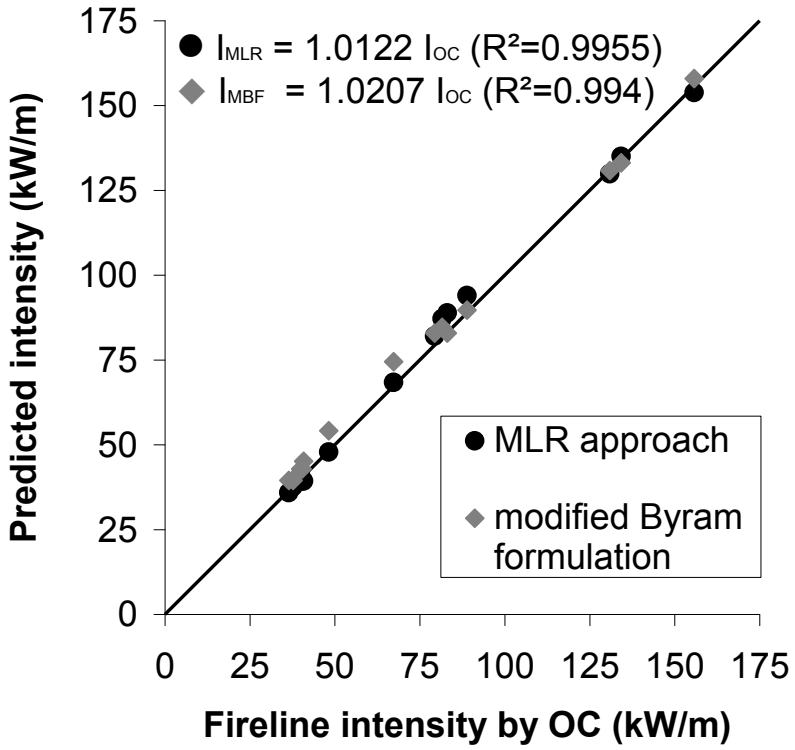

Fig. 6: Predictions of the mass loss rate approach and modified formulation of Byram intensity versus true fireline intensity measured by oxygen consumption calorimetry

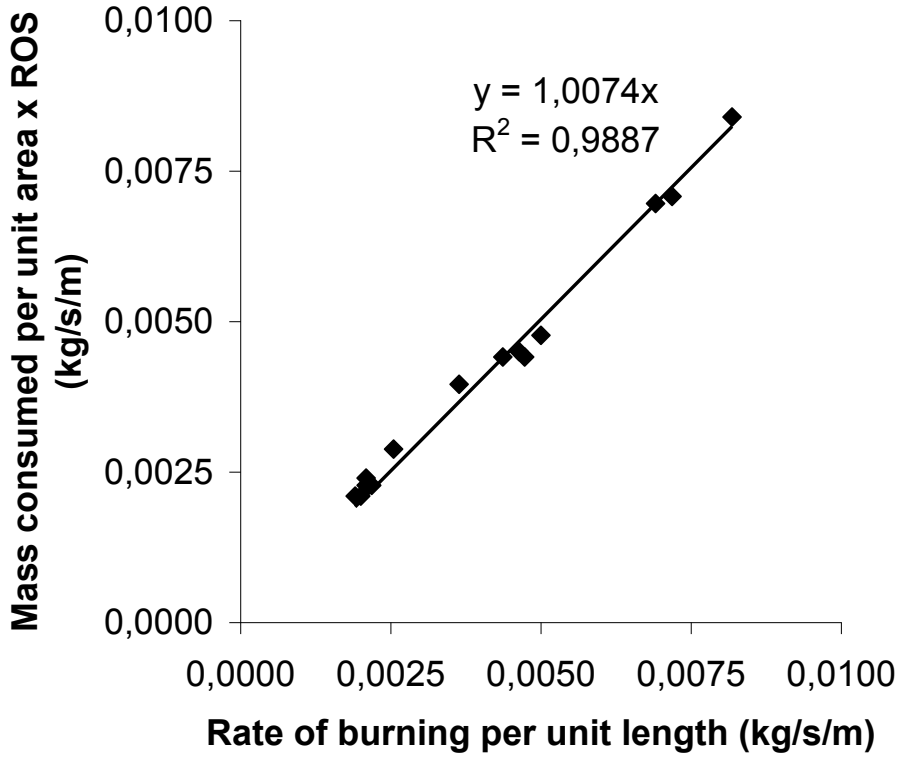

Fig. 7: Comparison of the rate of burning per unit length and the product of the mass consumed per unit area by the ROS

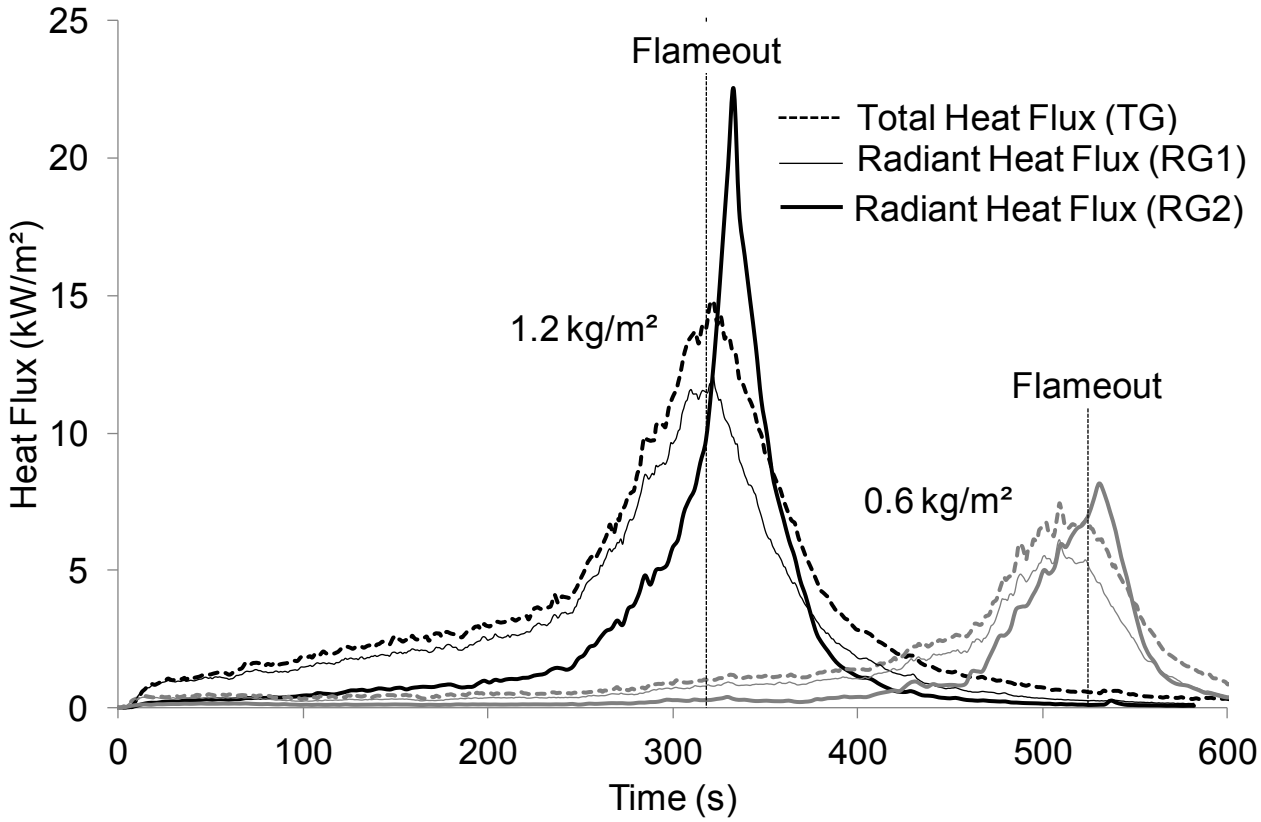

Fig. 8: Total and radiant heat fluxes

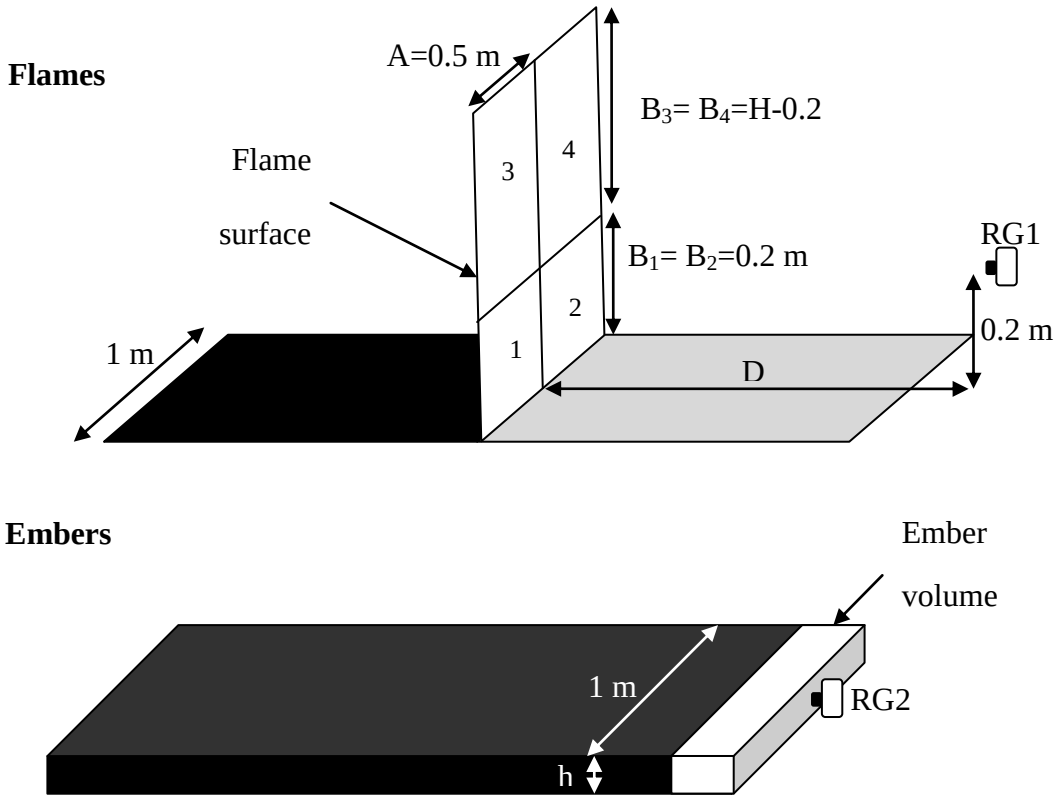

Fig. 9: Assumptions used for the determination of the view factors

List of Figure Captions

Fig. 1: Large Scale Heat Release Calorimeter.

Fig. 2: Geometric descriptors of the flame front.

Fig. 3: Fire front position and measurements of the mass versus time for 0.6 and 1.2 kg/m²

Fig. 4: Heat release rate and mass loss rate versus time for 0.6 and 1.2 kg/m²

Fig. 5: Fireline intensity versus rate of burning per unit length

Fig. 6: Predictions of the mass loss rate approach and modified formulation of Byram intensity versus true fireline intensity measured by oxygen consumption calorimetry

Fig. 7: Comparison of the rate of burning per unit length and the product of the mass consumed per unit area by the ROS

Fig. 8: Total and radiant heat fluxes

Fig. 9: Assumptions used for the determination of the view factors